JCB Journal of Cell Biology

REPORT

Ubiquitous membrane-bound DNase activity in podosomes and invadopodia

Kaushik Pal[1], Yuanchang Zhao[1], Yongliang Wang[1], and Xuefeng Wang[1,2]

Podosomes and invadopodia, collectively termed invadosomes, are adhesive and degradative membrane structures formed in many types of cells and are well known for recruiting various proteases. However, another major class of degradative enzymes, deoxyribonuclease (DNase), remains unconfirmed and not studied in invadosomes. Here, using surface-immobilized nuclease sensor (SNS), we demonstrated that invadosomes recruit DNase to their core regions, which degrade extracellular double-stranded DNA. We further identified the DNase as GPI-anchored membrane-bound DNase X. DNase recruitment is ubiquitous and consistent in invadosomes of all tested cell types. DNase activity exhibits within a minute after actin nucleation, functioning concomitantly with protease in podosomes but preceding it in invadopodia. We further showed that macrophages form DNase-active podosome rosettes surrounding bacteria or micropatterned antigen islets, and the podosomes directly degrade bacterial DNA on a surface, exhibiting an apparent immunological function. Overall, this work reports DNase in invadosomes for the first time, suggesting a richer arsenal of degradative enzymes in invadosomes than known before.

Introduction

Podosomes and invadopodia are micron-sized membrane protrusive structures that have both adhesive and degradative functions by interacting with the ECM (Chen et al., 1985; Dalaka et al., 2020; Tarone et al., 1985). They are found in a wide range of cell types, with podosomes formed in monocytes, osteoclasts, dendritic cells, smooth muscle cells, etc. and invadopodia formed in many carcinoma cells. Despite different origins, podosomes and invaodopodia share significant structural and enzymatic similarities (Albiges-Rizo et al., 2009). Both structures have actin cores surrounded by peripheral adhesion rings consisting of integrin, vinculin, paxillin, etc. (Badowski et al., 2008; Branch et al., 2012). In recent literature, these two structures were often collectively termed invadosomes (Linder et al., 2011; Saltel et al., 2011). As formed in various cell types, invadosomes are highly versatile and involved in many physiological processes, such as cell motility, cancer invasion and metastasis, matrix remodeling, and bone structure maintenance (Eddy et al., 2017; Poulter et al., 2015; Raynaud-Messina et al., 2018; Ridley, 2011).

One characteristic feature of invadosomes is their enzymatically degradative function. Matrix degradation by invadopodia has been correlated with cancer metastasis and invasion (Desai et al., 2008; Poincloux et al., 2009). In parallel, the degradative nature of podosomes has been considered as an important factor regulating the migration and tissue infiltration of macrophages (Cougoule et al., 2010; Linder et al., 1999; Van Goethem et al., 2011). Due to the physiological and pathological importance of their enzymatic functions, invadosomes have been pursued as pharmaceutical targets (Winer et al., 2018). Currently, the degradative ability of invadosomes is solely attributed to proteases such as serine proteases, ADAM proteases, and metalloproteases (Jacob and Prekeris, 2015; Lochter et al., 1998; Paz et al., 2014; Wagenaar-Miller et al., 2004). Surprisingly, DNase, another major class of degradative enzymes, has not been studied, identified, or even noticed in invadosomes.

In this work, we revealed that DNase is consistently and ubiquitously recruited to both podosomes and invadopodia. A surface-immobilized nuclease sensor (SNS; Wang et al., 2019), which maps DNase activity at the cell–substrate interface by fluorescence, was applied to study podosomes (in human and mouse macrophage-like cells and fish macrophages) and invadopodia (in human and mouse cancer cell lines). Results showed strong local DNase activity in both podosomes and invadopodia. Coimaging of structures and enzymatic activities in invadosomes confirmed that DNase is recruited quickly after the actin core nucleation in invadosomes and remains locally active at the core region. We further identified the DNase in invadosomes as DNase X (Shiokawa et al., 2007), a

[1]Department of Physics and Astronomy, Iowa State University, Ames, IA; [2]Molecular, Cellular, and Developmental Biology Interdepartmental Program, Iowa State University, Ames, IA.

Correspondence to Xuefeng Wang: xuefeng@iastate.edu.

glycosylphosphatidylinositol (GPI)–anchored membrane protein. We then devised a codegradation assay, by which we revealed that DNase and proteases are active concomitantly in podosomes, whereas DNase activity precedes protease activity in invadopodia. These results suggest that podosomes are equipped with more degradative enzymes than known so far. To our knowledge, this is the first report of DNase activity at the cell–substrate interface in invadosomes.

We then investigated the physiological function of DNase activity in podosomes in macrophages. On both *Escherichia coli*–immobilized surfaces and antigen micropatterned surfaces, macrophages patrolled on the surface by forming DNase-active podosomes in the cell front and quickly reacted to immunogenic targets by forming podosome rosettes around *E. coli* or antigen islets. We further show that podosomes in macrophages directly degrade bacterial DNA on the surface, demonstrating that macrophages can use podosomes to clean up extracellular pathogenic DNA without the need of internalizing it. We believe that this finding will be an important starting point to investigate more physiological functions of DNase in invadosomes.

Results and discussion

SNS reports DNase activity in invadosomes

Previous studies have discovered a plethora of adhesive, structural, and enzymatic proteins in invadosomes (Fig. 1 a; Buccione et al., 2004; Murphy and Courtneidge, 2011). Many proteases are known to take active roles in the function of invadosomes. DNase, as another major class of degradative enzymes, somehow remains unnoticed and uninvestigated in invadosomes. Here, we applied two DNase sensors and total internal reflection fluorescence (TIRF) microscopy to investigate the DNase activity in invadosomes at the cell–substrate interface. The first DNase sensor is surface-immobilized Cy3-labeled double-stranded DNA (dsDNA), as shown in Fig. 1 b. This sensor loses the dye if degraded by DNase and therefore reports DNase activity by fluorescence loss, resembling the classic dye-labeled gelatin degradation assay used to report protease activity of invadopodia (Berdeaux et al., 2004; Mueller et al., 1992). The other sensor is SNS (Fig. 1 c), a dsDNA labeled by a quencher–dye pair, and a biotin tag for surface immobilization. Initially dark SNS becomes fluorescent if the dsDNA is degraded and dye is freed from the quencher, hence reporting DNase activity at the cell–substrate interface by fluorescence gain. Human macrophage-like THP-1 cells activated with TGF-β1 (Rafiq et al., 2019) were plated on glass surfaces coated with these two types of sensors, respectively. On the surface coated with dye-labeled dsDNA, strong fluorescence loss in a punctate pattern was observed, colocalizing with podosomes that were identified by the actin cores and vinculin rings (Fig. 1, d and f). To rule out the possibility that these dark puncta were caused by local dye bleaching or sensor detachment, THP-1 cells were plated on an SNS-coated surface where podosomes produced bright fluorescence puncta, confirming that the dsDNA construct in the SNS was degraded (Fig. 1, e and g). These two assays confirmed that podosomes in THP-1 cells exhibit strong DNase activity in the core regions. Further verification was conducted to confirm that the DNase in the podosomes is dsDNA-specific (Fig. S1). Results showed that the DNase in podosomes degraded dsDNA regardless of DNA sequences but did not degrade single-stranded DNA (ssDNA) or DNA–peptide nucleic acid (PNA) hybrid duplex, which is supposed to be DNase resistant. As the SNS specifically responds to DNase activity, ruling out a potential false-positive signal caused by dye bleaching, we adopted the SNS platform for all following experiments.

We evaluated the consistency of DNase activity in podosomes. Coimaging of F-actin and DNase activity of THP-1 cells showed that 86 ± 5% of actin puncta are colocalized with SNS punctate signal. The experiment was conducted more than three times, and the percentage did not vary significantly. In the images, many SNS puncta have no corresponding actin cores. This is because invadosomes are subject to disassembly, while SNS surface records all historic DNase activity. As a result, there is a subset of SNS puncta where invadosomes have already disassembled.

DNase is ubiquitously recruited to invadosomes

To test if DNase is commonly recruited to invadosomes in different cell types, we applied the SNS assay to five cell types from different species, which form either podosomes or invadopodia: human macrophage-like THP-1, mouse macrophage-like RAW264.7, fish macrophages (identified in Fig. S2), MDA-MB-231 human breast cancer cells, and MTC (mouse musculus thyroid carcinoma) cells. Podosomes in RAW264.7 and THP-1 cells and fish macrophages were identified with imaging of actin cores. The latter two types of cells form invadopodia, which were identified with coimaging of actin, cortactin, and TKS5 (Fig. S3). All the five invadosome-forming cell lines exhibited significant DNase activity localized with the actin cores of invadosomes (Fig. 2, a–e), suggesting that DNase recruitment by invadosomes is highly consistent and ubiquitous in the different cell types and species. The SNS assay was also applied to CHO-K1 cells as a negative control (Uekita et al., 2001), which do not form podosomes or invadopodia. As expected, CHO-K1 cells did not form F-actin in a punctate pattern and exhibited no DNase activity on the SNS surface (Fig. 2 f). A statistical analysis shows that over 80% of podosomes in RAW264.7 and THP-1 cells and fish macrophages have exhibited DNase activities. The percentages of actin cores colocalizing with DNase activities in invadopodia are 80% in MDA-MB-231 and 46% in MTC, respectively (Fig. 2 g).

Temporal dynamics of DNase activity in podosomes

Podosomes and invadopodia have different temporal dynamics in terms of structures and functions. To investigate the temporal dynamics of the DNase activity relative to the structural formation of podosomes, we tested RAW264.7 cells stably transfected with LifeAct-GFP that reports F-actin on an SNS surface (Fig. 2 h and Video 1). Fluorescence time-lapse imaging was performed to monitor both the SNS signal and actin nucleation in live cells. Note that the emerging time of SNS signal is not the time of DNase recruitment, which may precede DNase activity reported by the SNS signal. Nonetheless, the result revealed that

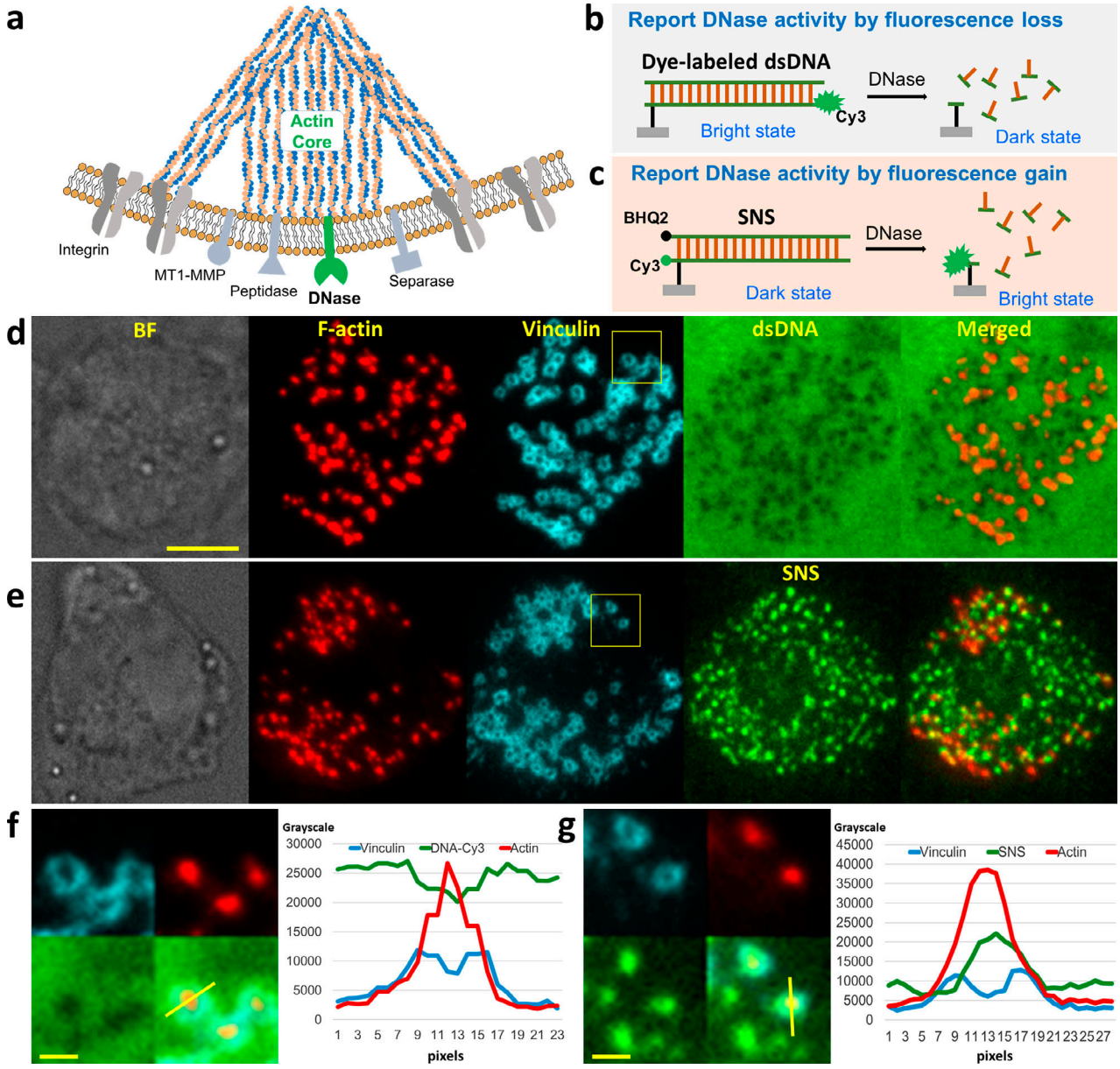

Figure 1. **DNase activity in invadosomes reported by SNS. (a)** Basic invadosome structure and representative proteins. DNase (depicted in green) is revealed in this study. **(b)** Surface-immobilized Cy3-labeled dsDNA visualizes DNase activity by fluorescence loss. **(c)** SNS with a quencher–dye pair reports DNase activity by fluorescence gain. **(d)** A THP-1 cell on a surface coated with Cy3-labeled dsDNA. Podosomes were identified by the characteristic actin core and vinculin ring. dsDNA was degraded in a dark punctate pattern colocalized with the podosomes. BF, bright field. **(e)** A THP-1 cell on an SNS-immobilized surface, which showed DNA degradation in a bright punctate pattern colocalized with podosomes. Statistics show that 86 ± 5% of actin puncta are colocalized with SNS punctate signal (600 podosomes over 20 cells). **(f and g)** Representative regions marked by yellow boxes in panels d and e, respectively. Line profiles (marked by yellow lines) of vinculin, F-actin, and DNase sensor signal in single podosomes are also presented in panels f and g. Scale bars represent 5 µm (d) and 1 µm (f and g).

the DNase activity in podosomes manifested quickly (within ~1 min) after the initiation of actin nucleation and remains active (Fig. 2, i and j) afterward. Further tests revealed that the actin core formation is required for DNase recruitment to podosomes, as inhibiting actin polymerization with cytochalasin D abolished DNase activity in the punctate pattern. In contrast, inhibiting myosin II (another important structural component) in podosomes with blebbistatin had an insignificant effect on DNase activity (Fig. S4).

DNase in invadosomes is GPI-anchored DNase X

The localized DNase activity in a punctate pattern suggests that the DNase in invadosomes is not secreted soluble protein but likely membrane bound. We hypothesized that the DNase in invadosomes is membrane-bound DNase X (Parrish et al., 1995), which is anchored to the membrane by a GPI linker (Paulick and Bertozzi, 2008). We first tested whether the DNase in invadosomes is GPI anchored. When treated with phosphatidylinositol-specific PLC (PI-PLC), which cleaves the GPI anchor, DNase activity in podosomes

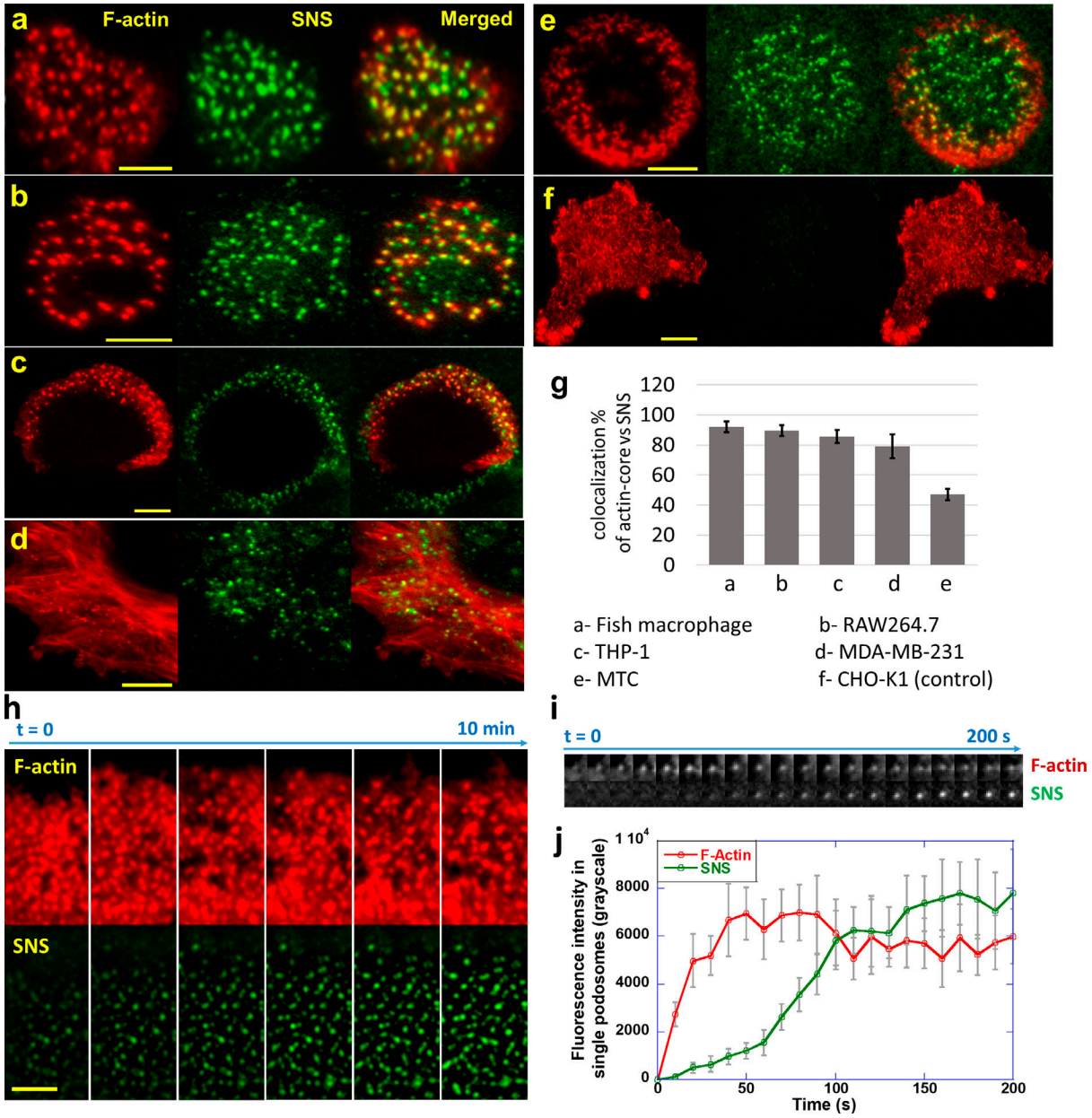

Figure 2. **Ubiquitous DNase activity in invadosome-forming cells. (a–e)** RAW264.7, THP-1, fish macrophages, MDA-MB-231, and MTC, with the former three forming podosomes and the latter two forming invadopodia, exhibited DNase activity in punctate patterns. **(f)** CHO-K1 cell as a control does not form invadosomes (no actin core), and no DNase activity was observed at the cell–substrate interface. **(g)** Percentage of actin cores that are colocalized with strong SNS punctate signal (20 cells for each data point, with 20–35 invadosomes analyzed for each cell). Error bars represent standard errors. **(h)** F-actin and SNS signal reporting DNase activity was coimaged in RAW264.7 cells transfected with LifeAct-GFP. **(i)** Time-series images of F-actin and SNS signal in one representative podosome (Video 1). The grid size is 2 × 2 μm^2. **(j)** Temporal curves of F-actin and DNase activity averaged over 20 podosomes, showing that DNase activity manifests in ∼1 min after actin core nucleation. Scale bars, 5 µm.

was significantly reduced, and SNS signal was nearly zero under the treatment of 5 U/ml PI-PLC (Fig. 3, a and b). The actin cores of podosomes remain unaltered in the treatment of PI-PLC. This result suggests that the DNase activity in podosomes is due to GPI-anchored nuclease, which is likely DNase X. We further tested by immunostaining if the DNase in podosomes is DNase X. The immunostained spots of DNase X and the SNS puncta are well colocalized (Fig. 3 c), suggesting that DNase X is recruited to podosomes. To further confirm the identity of the DNase, we knocked down DNase X expression in THP-1 cells with siRNA targeting human DNase X mRNA. DNase X knockdown significantly reduced the DNase X expression level in THP-1 cells (Fig. S5). With DNase X knocked down, DNase activity in podosomes of THP-1 cells also significantly decreased (Fig. 3, d and e), suggesting that DNase X is the major active DNase in podosomes. Collectively, we identified the DNase in podosomes as GPI-anchored DNase X.

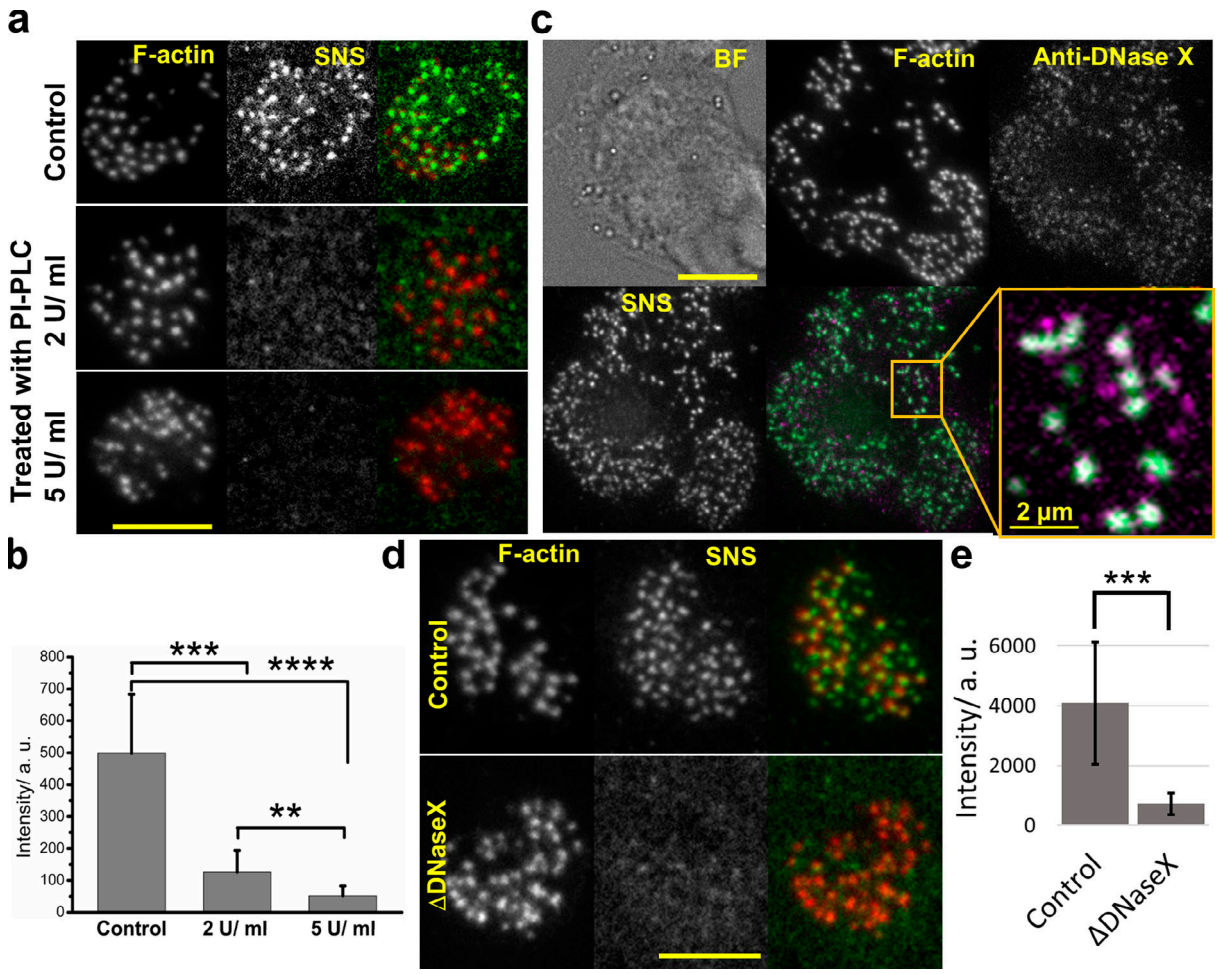

Figure 3. **Identification of the DNase in invadosomes. (a)** SNS and F-actin signals in THP-1 cells treated with PI-PLC, which cleaves GPI anchors. **(b)** SNS signals in THP-1 cells with 20 cells for each data point, showing that PI-PLC significantly reduced the DNase activity in invadosomes. The merged figure consists of SNS signal in green and anti-DNase X signal in magenta. **(c)** Immunostaining of THP-l cells with anti-DNase X showed good colocalization between anti-DNase X and SNS signal. **(d)** THP-1 with DNase X gene knockdown (ΔDNase) and the control cell on the SNS surfaces. Podosomes formed normally in both sets of cells. **(e)** THP-1 with DNase X gene knockdown showed a significant reduction of DNase activity reported by SNS signal. The analysis was based on 20 cells for each data point. All significance values were evaluated by two-tailed tests. **, P ≤ 0.01; ***, P ≤ 0.001; ****, P ≤ 0.0001. Error bars represent SD. Scale bars, 10 µm.

The capability of codegrading DNA and matrix proteins by invadosomes

Enzymatic degradation is the crucial and prominent biochemical functionality of invadosomes. Previously, extensive research has been dedicated to investigating the degradation of ECM proteins by invadosomes (Berdeaux et al., 2004; Kelly et al., 1994). However, ECM also consists of extracellular DNA originating from apoptotic and necrotic cells, neutrophil extracellular traps (Brinkmann et al., 2004), invading pathogens, etc. (Aucamp et al., 2018; Brinkmann et al., 2004). Here, we designed a co-degradation assay to simultaneously monitor the degradation of both matrix protein and extracellular DNA by invadosomes. We coated glass surfaces with both SNS and dye-labeled (Hy-Light488) fibronectin (FN) and tested THP-1 and MTC cells on these surfaces. Time-lapse fluorescence imaging showed that podosomes were formed in THP-1 cells and rapidly degraded both SNS (made of dsDNA) and FN nearly simultaneously (Fig. 4, a and b; and Video 2). This suggests that DNase may potentially participate in matrix degradation, with an enzymatic role parallel to that of proteases. In contrast, invadopodia formed in MTC cells exhibited rapid DNase activity, but no degradation of FN (due to protease activity) was observed within 1 h (Fig. 4, c and d; and Video 3). A previous study showed that invadopodia exhibited detectable protease activity on the gelatin surface within 1 h (Artym et al., 2006). This discrepancy may be due to the fact that our assay was performed on the rigid glass surface, where invadopodia may have longer maturation time than those on the soft gel surface. Nonetheless, this experiment suggests that DNase activity manifests more rapidly than protease activity in invadopodia. To confirm that this effect is statistically significant, we repeated this test with imaging over a larger number of fixed cells on surfaces coated with SNS and FN. The result is consistent with the result of live-cell experiments. Podosomes in THP-1 cells degraded both dsDNA and FN, whereas invadopodia in MTC only degraded dsDNA (Fig. 4, e and f). Overall, our results suggest that DNase activity is more

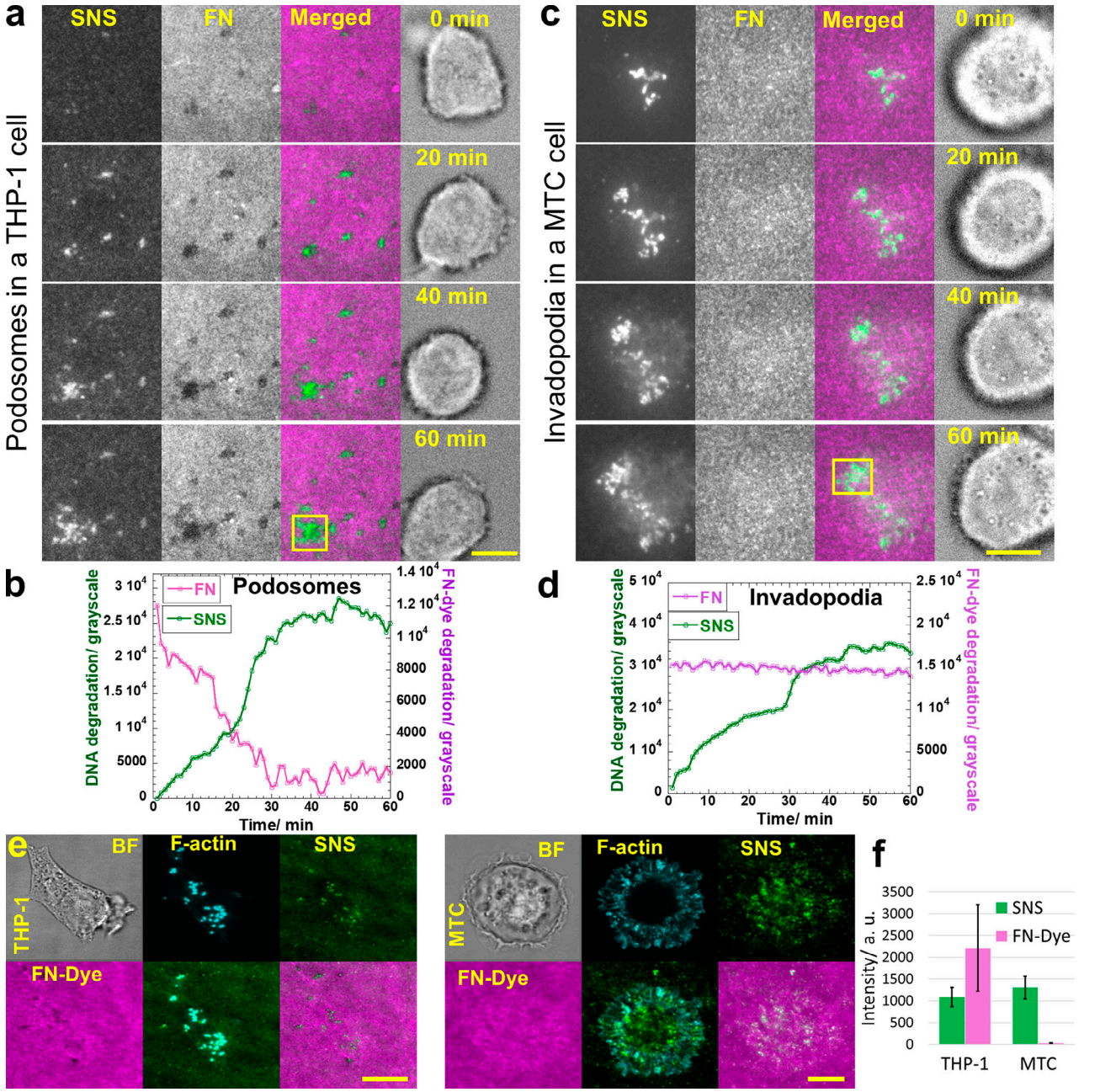

Figure 4. **Codegradation of SNS (extracellular DNA) and HyLite488-labeled FN (matrix protein) by invadosomes. (a)** A podosome forming THP-1 cell was imaged over 60 min on a surface coated with both SNS and HyLite488-labeled FN (Video 2). **(b)** Fluorescence intensity analysis shows that the degradation of both SNS and FN is starting at a similar time by podosome. **(c)** Invadopodia forming MTC cell on a surface coated with both SNS and HyLite488-labeled FN (Video 3). **(d)** Fluorescence intensity analysis shows that only SNS was degraded by invadopodia; no degradation of FN was observed within the time frame of the experiment. **(e)** THP-1 and MTC with immunostained F-actin on surface, coated with SNS and FN dye. **(f)** DNase activity and protease activity in invadopodia (in MTC cells) and podosomes (in THP-1 cells). Statistical analysis was based on 20 cells. Error bars represent SD. Scale bars, 10 µm.

ubiquitous and prompter than protease activity in invadosomes, potentially making it a superior biomarker for the identification of invadosomes and also suggesting that DNase may play a prominent physiological role in invadosomes.

DNase-active podosome rosettes target and surround surface-immobilized *E. coli*

As invadosomes are formed in various cell types, the function of DNase in invadosomes is likely versatile. Here, we studied the physiological role of DNase in macrophages that form rich podosomes. Because the main function of macrophages is to serve as an immune defense to ingest invading pathogens, which potentially carry pathogenic DNA, we studied DNase activity in podosomes with the presence of pathogens and immunogenic materials. On an SNS surface, a macrophage-like cell (THP-1) formed podosomes at cell peripheral region and constantly degraded surface-immobilized DNA, probing and patrolling on the surface (Fig. 5 a and Video 4). When encountering pathogens

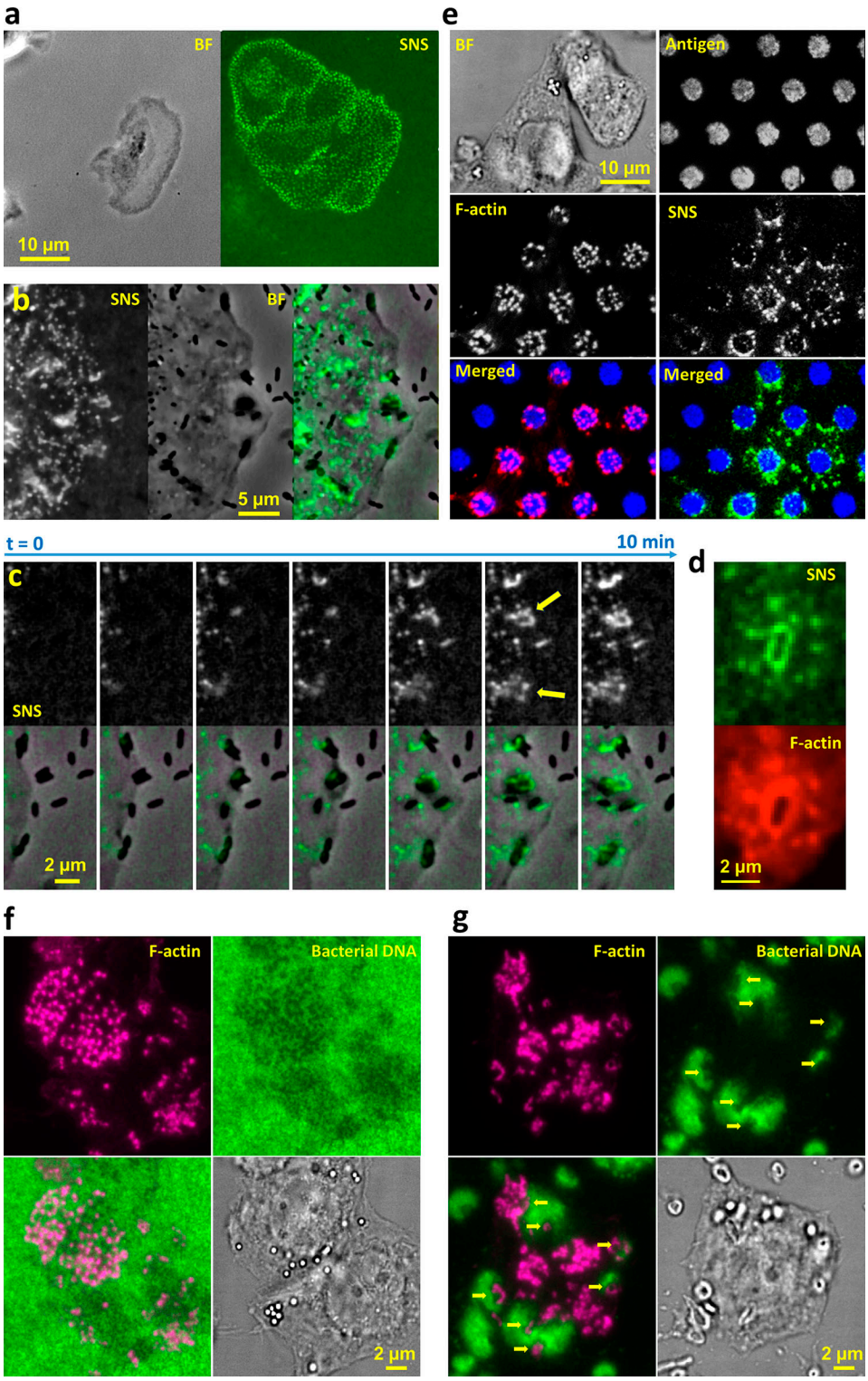

Figure 5. **DNase-active podosomes respond to pathogens and immunogenic material. (a)** A migrating macrophage-like cell (THP-1) formed dense podosomes in the leading edge and degraded the surface DNA along the path (Video 4). **(b)** A macrophage-like cell (THP-1) specifically reacted to surface-immobilized *E. coli* (dark short rod-like objects) with DNase activity (Video 5). **(c)** DNase-active podosomes formed around surface-immobilized *E. coli* in a rosette pattern (yellow arrows), degrading the local extracellular DNA (SNS), until *E. coli* was internalized. **(d)** Coimaging of SNS signal and F-actin of a THP-1 cell around a bacterium. **(e)** THP-1 cells formed podosome rosettes around the antigen (donkey IgG) islands (size, 5 µm) and degraded the surrounding surface DNA, showing general reaction to the immunogenic material by forming DNase-active podosomes. Note that SNS was not coated on the IgG islands but was coated in the background. **(f)** DNase-active podosomes degrade bacterial DNA. THP-1 cells on a surface uniformly coated with bacterial DNA extracted from *E. coli*. DNA was stained with Sytox green. **(g)** A THP-1 cell on a surface decorated with chromosomal DNA spilled by individual *E. coli* lysed on site. Arrows indicate the DNA degrading sites. DNA was stained with Sytox green.

(*E. coli* immobilized on the SNS surface), podosomes and DNase immediately targeted the pathogens and started reacting around them (Fig. 5 b and Video 5). Eventually, podosomes formed in a rosette pattern around the immobilized *E. coli* (Fig. 5 c), while DNase in the podosomes degrades extracellular DNA (the SNS) in the peripheral region around *E. coli*, until *E. coli* were engulfed by the macrophage. Coimaging of SNS signal and F-actin stained by phalloidin confirmed that the SNS signal of THP-1 cells around *E.* coli originated from podosomes (Fig. 5 d). This assay revealed that DNase-active podosomes preferentially form around pathogens, suggesting that podosomes in macrophages may have a direct role in targeting and engaging pathogens and destroying DNA in the proximity of the pathogens.

DNase-active podosomes form around antigen islets

To further confirm that the formation of podosomes and DNase activity around pathogenic targets are specific immune responses, we tested THP-1 cells on a glass surface printed with micron-sized antigen islets (donkey IgG) and coated with SNS in the background. The whole surface was also coated with poly-L-lysine (PLL) to assist THP-1 cell adhesion. IgG is a foreign substance that can elicit an immune reaction in macrophages (Arend and Mannik, 1973). Coimaging of F-actin and DNase activity showed that DNase-active podosomes are indeed preferentially formed around antigen islets (Fig. 5 e), suggesting that podosome formation and the associated DNase activity were purposed immune responses. Collectively, we demonstrated that DNase activity in podosomes targets and surrounds immunogenic sources, possibly functioning as a defense mechanism by degrading potential foreign genetic material carried by pathogens. This study shows the immunological implications of podosomes in macrophages and suggests that DNase in podosomes could be the first-line weaponry destroying genetic material originating from pathogens.

Podosomes degrade bacterial DNA extracellularly by contact

As we demonstrated that macrophages preferentially form podosomes on immunogenic materials, we further tested whether these podosomes are capable of degrading pathogenic DNA directly without the need of internalizing it. First, we extracted crude DNA from *E. coli* and immobilized the DNA uniformly on a glass surface (see Materials and methods). THP-1 cells activated with TGF-β1 were plated on the surface. After 1 h of incubation, cells were fixed and permeabilized, and Sytox green was used to stain bacterial DNA on the surface. TIRF imaging showed that the majority of podosomes degraded the surface-immobilized DNA, suggesting that podosomes in macrophages can degrade bacterial DNA immobilized on a surface (Fig. 5 f). To further demonstrate that podosomes can directly degrade chromosomal DNA released by pathogens, we immobilized *E. coli* on a surface and lysed them on site with lysozyme. Chromosomal DNA was spilled out from individual *E. coli* and immobilized locally on the surface. Activated THP-1 cells were cultured on the surface and shown to degrade bacterial chromosomal DNA on the surface (Fig. 5 g, indicated by the yellow arrows). Collectively, these experiments showed that podosomes in macrophages are able to degrade pathogenic DNA extracellularly, revealing an important yet unreported role of DNase-active podosomes in immune response and extracellular DNA cleanup.

Conclusion

In summary, we reported DNase activity in both podosomes and invadopodia, characterized its temporal dynamics, and confirmed its identity. The DNase activity in invadosomes is strong, prompt, localized, and ubiquitous in invadosomes across different cell types and species, suggesting that invadosomes generally recruit DNase. We then identified it as membrane-bound DNase X. The DNase X may work with proteases in parallel to degrade ECM, which consists of both matrix proteins and extracellular DNA released by dead cells and pathogens (Aucamp et al., 2018; Brinkmann et al., 2004). DNase activity is more consistent than protease activity in invadosomes, potentially making it a more robust biomarker of invadosomes. The presence of DNase in invadosomes also provides new therapeutic targets and cautions for researchers in performing gene-based therapeutics to invadopodium-forming cancer cells.

The ubiquitous DNase activity in invadosomes suggests that its function is likely versatile. Here, we preliminarily investigated the immunological role of DNase activity in podosomes of macrophages. Our results showed that the DNase-active podosomes preferentially form around micron-sized antigen islets and pathogens. We further showed that podosomes in macrophages are indeed capable of degrading pathogenic DNA by contact, without the need of DNA internalization. Collectively, podosome formation elicited by immunogenic sources and pathogenic DNA degradation is caused by podosomal DNase, suggesting that podosomal DNase plays an important role in immune surveillance, defense, and extracellular DNA cleanup. Invadosomal DNase has likely more physiological functions than shown in this work, as its presence is ubiquitous in invadosomes, which are formed in many cells, including metastatic cancer cells and matrix-remodeling cells (osteoblasts). The trafficking of DNase X to invadosomes also awaits further study to reveal whether DNase X recruitment is triggered by extracellular DNA (including SNS itself) and how cells recruit DNase X to invadosomes.

Overall, revealing DNase in invadosomes adds an important piece to the whole picture of enzymatic behaviors in these dynamic and versatile structures. To the best of our knowledge, this is the first report of DNase activity in invadosomes since their discovery decades ago. The absence of DNase study in invadosomes in the past could be due to the lack of a sensor that can image DNase activity at the cell–substrate interface. This work will likely encourage more research to study the physiological roles of DNase in invadosomes and the associated signaling pathways, and the DNase sensor SNS could be a valuable tool to bring DNase activity to light.

Materials and methods

Synthesis of SNS

We customized and ordered oligonucleotides from Integrated DNA Technologies with sequences and modifications as follows: DNA 1, 5′-GGGCGGCGACCTCAGCAT-3′/3BHQ_2/; DNA 2, /5BiosG/

T/iCy3/5′-ATGCTGAGGTCGCCGCCC-3′/; DNA 3, 5′-GGGCGGCGACCTCAGCAT-3′; DNA 4, /5Cy3/5′-AGGTCGATGCTGCCGCCC-3′/3Bio/.

For the construction of SNS, DNA 1 and DNA 2 dissolved in 1× PBS were annealed at a molar ratio of 1.2:1.0 and stored at 4°C at a final concentration 10 µM for further use. For the construction of Cy3-labeled DNA, DNA 3, and DNA 4 were annealed in the same conditions as SNS annealing.

DNA and PNA used in Fig. S1

All DNA sequences are as follows: ssDNA, /5Biosg/5′-ATGCTGAGGTCGCCGCCC-3′/Cy3/; CpG-free: 5′-GGCACCCAGGCACCACCC-3′/3BHQ_2/; /5Biosg/T/iCy3/5′-GGGTGGTGCCTGGGTGCC-3′; other sequence, 5′-GGGAGGACGGAGCAGGGC-3′/3BHQ_2/; /5Biosg/T/iCy3/5′-GCCCTGCTCCGTCCTCCC-3′; PNA/DNA: 5′-GGGCGGCGACCTCAGCAT-3′/3BHQ_2/; Biotin-OO-Lys(Cy3)-O-5′-ATGCTGAGGTCGCCGCCC-3′.

SNS immobilization on the glass surface

The imaging platform for our study is the SNS-immobilized glass surface. To prepare this surface, we followed three steps. In step 1, a solution of 200 µg/ml BSA-biotin (biotin-conjugated BSA, A8549; Sigma-Aldrich) and 2 µg/ml FN (1918-FN; R&D Systems) in PBS buffer was incubated on a glass-bottom Petri dish (D35-14-1.5-N; in vitro Scientific) for 30 min at 4°C. Both BSA and FN can be physically adsorbed on the glass surface. FN was used for assisting cells in adhering. The surface was rinsed with cold PBS thrice. In step 2, the surface was incubated with a solution of 50 µg/ml neutravidin (31000; Thermo Fisher Scientific) in PBS for 30 min at 4°C and rinsed with cold PBS thrice. In step 3, the surface was incubated with a solution of 0.1 µM SNS in PBS for 30 min at 4°C and rinsed with PBS thrice. The glass surface became ready for cell plating and further experiments.

FN-HiLyte 488 surface preparation

A solution of 5 µg/ml FN labeled with HiLyte fluor 488 (FNR02-A; Cytoskeleton) in PBS was incubated on a glass-bottom Petri dish for 30 min at 4°C and rinsed with cold PBS thrice. The Petri dish was further coated with 200 µg/ml BSA-biotin, 50 µg/ml neutravidin, and 0.1 µM SNS consecutively and became ready for experiments.

Cell culture and cell plating

Both cancer (MDA-MB-231 and MTC) and noncancer macrophage-resembling (RAW264.7 and THP-1) cell lines were used in SNS assays. All cell lines were cultured according to the supplier's protocol. Macrophage activation was done with treatment of 1 ng/ml lipopolysaccharide (L2630; Sigma-Aldrich) to RAW264.7 cells or 2 ng/ml TGF-β1 (240-B/CF; R&D Systems) to THP-1 cells for 24–36 h, respectively. RAW264.7 cells were stably transfected with LifeAct-GFP. For experiments, cells were harvested at 80–90% confluency using the following method: After removing the culture medium, cells were first washed and incubated with cell detaching solution inside the CO_2 incubator for 5–7 min. The recipe for 1 liter cell detaching solution is 100 ml 10×HBSS + 10 ml 1 M Hepes + 10 ml 7.5% sodium bicarbonate + 2.4 ml 500 mM EDTA. The rest of the volume was made up by distilled water, and the pH was adjusted to 7.4. Cells were gently pipetted off from the Petri dish, transferred into a 1.5-ml centrifuge tube, and centrifuged for 3 min at 300 *g*. Cell pellet was resuspended with the corresponding complete medium. The solution was then transferred on the glass surface modified with SNS and incubated for 30–60 min inside a CO_2 incubator before imaging.

Fish macrophage extraction

We developed a convenient method to extract a small amount of fish macrophages from fish scales. One or two scales were plucked from a fantail goldfish (*Carassius auratus*) using a flat-tip tweezers and placed on a glass-bottom Petri dish with the interior side of the scales contacting the glass surface. After 1–2 min, culture medium (IMDM, 30–2005; ATCC USA) spiked with 20% fetal bovine serum and 1% penicillin was added. The scales were incubated at room temperature for ∼12–24 h to allow cells to migrate out. Before experiments, cells were detached from the Petri dish using EDTA solution and then harvested by centrifuging (300 *g* for 3 min) and resuspending in culture medium. The cell solution was incubated on an SNS surface for 1 h. Maintenance of goldfish for the experiment was performed under the supervision of Institutional Animal Care and Use Committee (log number 8–16-8333-I).

Previously, this method was used to harvest keratocytes, a type of fast-migrating cells functioning in wound healing. However, we found 10–30% cells extracted from the fish scales are actually macrophages (identified by TNF-α immunostaining), not keratocytes. These two cell types are distinctly different in terms of migration rate, podosome formation, and surface DNA degradation. Keratocytes migrate at 10–20 µm/min, do not form podosomes, and produce no DNA degradation signals. On SNS surfaces, macrophages can be simply identified with DNA degradation in punctate patterns.

Immunostaining

Immunostaining began with the fixation of cells with 4% formaldehyde solution in PBS for 15 min at room temperature. After removing the formaldehyde solution, cells were permeabilized with 0.1% Triton X-100 solution in PBS for 20 min at room temperature. Then the cells were blocked with 5 mg/ml BSA solution in PBS for 45 min at room temperature. For the staining of actin, phalloidin–Alexa Fluor 405 (A30104; Thermo Fisher Scientific) was used, and the sample was incubated according to the supplier's instruction and washed with PBS three times with 5 min each. For the staining of vinculin or DNase X, cell samples were first treated with primary antibodies, including anti-vinculin (90227; Millipore), anti-TKS5 (MABT336; Millipore), anti-TNF-α (ab1793; Abcam), or anti-DNase X (H00001774-MO2; Abnova), in PBS for 1 h at room temperature and then washed with PBS three times. PBS remained on the samples for 5 min before its removal. The samples were then treated with dye-labeled secondary antibody (ab175660; Abcam) solution in PBS, incubated for 1 h at room temperature, and washed thrice with PBS with a 5-min incubation time. Cortactin staining was performed with dye-labeled anti-cortactin (05–180-AF647; Millipore).

Cell transfection

For transfection, corresponding cells were cultured in a 35-mm Petri dish up to 70–80% of confluency. Plasmid DNA (2–3 µg) was diluted in 400 µl Opti-MEM (11058021; Thermo Fisher Scientific) spiked with 2–3 µl Plus reagent (15338100; Thermo Fisher Scientific). The plasmid solution was mixed and incubated for 10 min at room temperature. After that, 6–8 µl Lipofectamine-LTX (15338100; Thermo Fisher Scientific) was added to the plasmid solution, which was then mixed and incubated at room temperature for 30 min. The medium in a Petri dish of cells was exchanged with 2 ml fresh complete medium added with the plasmid mixture. Cells were incubated in an incubator for 18–24 h. Before experiments, cells were detached with EDTA solution and plated on the imaging platform.

Inhibitor study

For GPI inhibition, THP-1 cells activated by 2 ng/ml TGF-β1 for 36–48 h were plated on the SNS imaging plate along with 2 or 5 U/ml of PI-PLC (P8804; Sigma-Aldrich) in complete growth medium for 1 h and then stained with phalloidin–Alexa Fluor 405 before imaging. For other inhibitors, activated cells were detached from the surface with EDTA treatment and then centrifuged in a centrifuge tube. The pellet was resuspended in complete medium with desired concentrations of the inhibitors blebbistatin (B0560; Sigma-Aldrich) and cytochalasin D (C8273; Sigma-Aldrich). The cell suspensions with inhibitors were plated on the imaging substrate and incubated in CO_2 incubator before imaging.

siRNA-mediated DNase X knockdown

THP-1 cells were harvested, resuspended in serum-free RPMI medium, and plated in a 24-well plate (800 µl per well). For transfection of DNase X siRNA (sc-77165; Santa Cruz Biotechnology), 2 µl of 10 µM siRNA and 2 µl Lipofectamine RNAiMAX (13778100; Thermo Fisher Scientific) were added to 200 µl Opti-MEM (31985062; Thermo Fisher Scientific) and incubated for 15 min. The mixture was then added to the cell suspension. After 24 h, medium of the transfected cells and control cells was replaced with complete RPMI medium spiked with TGF-β1 at 2 ng/ml concentration. After 48 h, these cells were plated on SNS-coated surfaces and incubated for 90 min in an incubator with 5% CO_2. F-actin immunostaining was performed for the identification and quantification of DNase activity. Cells were imaged by a TIRF microscope, and results were analyzed with 20 cells from both the control group and the transfected cell group.

Immobilization of *E. coli* on SNS surfaces

The immobilization of the *E. coli* (DH10B) was performed in following steps. First, the glass-bottom Petri dish was coated with 1 µg/ml PLL (P7890; Sigma-Aldrich) in milli-Q water for 30 min and washed thrice with milli-Q water. *E. coli* was harvested by three cycles of centrifuging (10,000 relative centrifugal force), discarding supernatant, and resuspending in milli-Q water. Bacteria solution after density adjustment was transferred onto the PLL-coated Petri dish and incubated for 30 min at room temperature. The *E. coli*–immobilized PLL surface was washed thrice with milli-Q water, and we continued to perform SNS coating according to the above-described method.

IgG micropatterning

The glass-bottom Petri dish was first coated with 10 µg/ml PLL in milli-Q water for 30 min and then washed with milli-Q water three times. The surface was blown to dry with a stream of compressed air. A drop of 10 µl solution (100 µg/ml) of donkey anti-rabbit IgG conjugated with Alexa Fluor 405 (ab175651; Abcam) was placed onto a clean glass slide, and a Polydimethylsiloxane stamp (5 µm diameter, 10 µm spacing and 5 µm pillar height for each dot, Research Micro Stamps) was placed onto the droplet (facing the micropatterned surface toward the droplet) and incubated for 10 min. The stamp was then taken off the antigen-solution droplet, and residual liquid on the stamp was blown off with compressed air. The stamp was placed onto the PLL surface for 10 min and carefully retracted afterward. Note that the stamp should not have horizontal motion relative to the PLL surface to avoid smearing the surface. The surface was washed with milli-Q water thrice, and SNS coating was performed on the surface according to usual method.

THP-1 cells on bacterial DNA purified from *E. coli*

50 µg/ml PLL in water was added to the well of a glass-bottom Petri dish and incubated for 20 min at room temperature. The Petri dish was washed with water three times. DNA was extracted from *E. coli* using a high-speed plasmid mini kit (IB47101; IBI Scientific) and immobilized on the PLL-coated glass surface. The immobilization is enabled by the electrostatic force, as the PLL coating is positively charged and DNA backbone is negatively charged. 350 ng/µl DNA solution in elution buffer (of the kit) was placed on the PLL-coated Petri dish, incubated for 30 min at the room temperature, and then washed with PBS three times. THP-1 cells were plated in the Petri dish and incubated for 1 h in an incubator (5% CO_2 and 37°C). The cells were then fixed and permeabilized with 4% formaldehyde and 0.2% Triton X-100 solution, respectively. F-actin and extracellular DNA were stained with phalloidin–Alexa Fluor 647 (A22287; Thermo Fisher Scientific) and Sytox green (S34862; Thermo Fisher Scientific), respectively, with a 20-min staining time. Note that Sytox green should not be applied before THP-1 cell incubation, as Sytox green may block the DNase–DNA interaction.

THP-1 cells on locally immobilized DNA from individual *E. coli*

Freshly cultured *E. coli* were harvested by centrifuging (6,000 relative centrifugal force for 1 min) in a 1.5-ml centrifuge tube. The pellet was resuspended in water and recentrifuged for three times. *E. coli* suspended in water was then added on the PLL-coated Petri dish (detailed in previous paragraph) and incubated for 30 min at room temperature. *E. coli* should be immobilized on the glass surface. The surface was washed with water for three times. Next, 0.5 mg/ml lysozyme (L6876; Sigma-Aldrich) in 25 mM Tris-HCL buffer (pH 8.0 with 50 mM glucose and 10 mM EDTA) was added to the Petri dish and incubated at 37°C for 4 h to lyse the *E. coli* on site. The surface was washed with PBS three times. Chromosomal DNA from individual *E. coli* was

spilled out and immobilized locally on the PLL surface. THP-1 cells were then plated on the Petri dish and incubated for 1 h in an incubator (5% CO_2 and 37°C). Cells were fixed and permeabilized with 4% formaldehyde and 0.2% Triton X-100 solution, respectively. F-actin and extracellular DNA were stained with phalloidin–Alexa Fluor 647 and Sytox green, respectively, by incubating for 20 min at room temperature.

Microscopy and image processing

All static and time-lapse imaging was performed using TIRF microscopy setup (Nikon Ti-2) with a 100× oil immersion objective (TIRF 100X, NA = 1.49). An electron-multiplying charge-coupled device Andor DU-897 X-11940 (model IXON-L-897) camera was used as the detector. Images and data were analyzed by a MATLAB code developed in our laboratory (Data S1). All fixed sample imaging was done at room temperature and live-cell imaging at 37°C. The wavelengths of laser as the excitation light were selected as 405, 488, 561, and 640 nm for corresponding fluorophores. The image acquisition software provided with microscope (NIS-Element AR 5.11.00) was used to acquire all images.

Statistical methods

The main body of data in this paper is in the format of images and videos. Quantification of fluorescence intensities of target signals in these images and videos was performed with a MATLAB code that we compiled. The code allows us to read images or videos produced by the microscope in a computer, and it manually selects single-podosome regions on which the fluorescence intensities of F-actin, SNS, or other signals are quantified. The MATLAB code is provided as a supplemental file (Data S1). The graphs for data presentation were prepared with Kaleidagraph software. P values were evaluated with two-tailed test with the command "ttest" in MATLAB. Data distributions were generally assumed to be normal, but they were not formally tested.

Online supplemental material

Fig. S1 shows that podosomes in THP-1 cells degraded dsDNA regardless of their sequences but degraded neither ssDNA nor PNA–DNA hybrid. Fig. S2 shows the identification of fish macrophages using TNF-α immunostaining. Fig. S3 shows the colocalization of cortactin and F-actin in MTC and MDA-MB-231 cells and the colocalization of TKS5 and F-actin in MDA-MB-231 cells. Fig. S4 shows that DNase activity in podosome depends on actin polymerization, but not myosin II. Fig. S5 Shows that siRNA knockdown reduced the expression level of DNase X in THP-1 cells. Video 1 shows real-time DNase activity and actin core nucleation in a LifeAct-GFP–transfected RAW264.7 cell on an SNS surface. Video 2 shows DNA and matrix protein codegradation by a THP-1 cell. Video 3 shows DNA and matrix protein codegradation by an MTC cell. Video 4 displays a migrating macrophage degrading extracellular DNA on an SNS surface by podosomes in the cell front. Video 5 shows a THP-1 cell reacting to *E. coli* by forming DNase-active podosomes around *E. coli*. Data S1 contains the MATLAB code.

Acknowledgments

We thank Dr. Kaitlin Bratlie (Iowa State University, Ames, IA) for sharing the RAW264.7 cell line and Dr. Ian Schneider (Iowa State University, Ames, IA) for sharing the MTC cell line.

This work was supported by the National Science Foundation (1825724) and the National Institute of General Medical Sciences (1R35GM128747).

The authors declare no competing financial interests.

Author contributions: X. Wang and K. Pal conceived the project. K. Pal, Y. Zhao, and Y. Wang performed the experiments. K. Pal, Y. Zhao, and X. Wang analyzed the data. X. Wang and K. Pal wrote the manuscript.

Submitted: 14 August 2020
Revised: 2 December 2020
Accepted: 5 April 2021

References

Albiges-Rizo, C., O. Destaing, B. Fourcade, E. Planus, and M.R. Block. 2009. Actin machinery and mechanosensitivity in invadopodia, podosomes and focal adhesions. *J. Cell Sci.* 122:3037–3049. https://doi.org/10.1242/jcs.052704

Arend, W.P., and M. Mannik. 1973. The macrophage receptor for IgG: number and affinity of binding sites. *J. Immunol.* 110:1455–1463.

Artym, V.V., Y. Zhang, F. Seillier-Moiseiwitsch, K.M. Yamada, and S.C. Mueller. 2006. Dynamic interactions of cortactin and membrane type 1 matrix metalloproteinase at invadopodia: defining the stages of invadopodia formation and function. *Cancer Res.* 66:3034–3043. https://doi.org/10.1158/0008-5472.CAN-05-2177

Aucamp, J., A.J. Bronkhorst, C.P.S. Badenhorst, and P.J. Pretorius. 2018. The diverse origins of circulating cell-free DNA in the human body: a critical re-evaluation of the literature. *Biol. Rev. Camb. Philos. Soc.* 93:1649–1683. https://doi.org/10.1111/brv.12413

Badowski, C., G. Pawlak, A. Grichine, A. Chabadel, C. Oddou, P. Jurdic, M. Pfaff, C. Albigès-Rizo, and M.R. Block. 2008. Paxillin phosphorylation controls invadopodia/podosomes spatiotemporal organization. *Mol. Biol. Cell.* 19:633–645. https://doi.org/10.1091/mbc.e06-01-0088

Berdeaux, R.L., B. Díaz, L. Kim, and G.S. Martin. 2004. Active Rho is localized to podosomes induced by oncogenic Src and is required for their assembly and function. *J. Cell Biol.* 166:317–323. https://doi.org/10.1083/jcb.200312168

Branch, K.M., D. Hoshino, and A.M. Weaver. 2012. Adhesion rings surround invadopodia and promote maturation. *Biol. Open.* 1:711–722. https://doi.org/10.1242/bio.20121867

Brinkmann, V., U. Reichard, C. Goosmann, B. Fauler, Y. Uhlemann, D.S. Weiss, Y. Weinrauch, and A. Zychlinsky. 2004. Neutrophil extracellular traps kill bacteria. *Science.* 303:1532–1535. https://doi.org/10.1126/science.1092385

Buccione, R., J.D. Orth, and M.A. McNiven. 2004. Foot and mouth: podosomes, invadopodia and circular dorsal ruffles. *Nat. Rev. Mol. Cell Biol.* 5:647–657. https://doi.org/10.1038/nrm1436

Chen, W.T., J.M. Chen, S.J. Parsons, and J.T. Parsons. 1985. Local degradation of fibronectin at sites of expression of the transforming gene product pp60src. *Nature.* 316:156–158. https://doi.org/10.1038/316156a0

Cougoule, C., V. Le Cabec, R. Poincloux, T. Al Saati, J.L. Mège, G. Tabouret, C.A. Lowell, N. Laviolette-Malirat, and I. Maridonneau-Parini. 2010. Three-dimensional migration of macrophages requires Hck for podosome organization and extracellular matrix proteolysis. *Blood.* 115:1444–1452. https://doi.org/10.1182/blood-2009-04-218735

Dalaka, E., N.M. Kronenberg, P. Liehm, J.E. Segall, M.B. Prystowsky, and M.C. Gather. 2020. Direct measurement of vertical forces shows correlation between mechanical activity and proteolytic ability of invadopodia. *Sci. Adv.* 6:eaax6912. https://doi.org/10.1126/sciadv.aax6912

Desai, B., T. Ma, and M.A. Chellaiah. 2008. Invadopodia and matrix degradation, a new property of prostate cancer cells during migration and invasion. *J. Biol. Chem.* 283:13856–13866. https://doi.org/10.1074/jbc.M709401200

Eddy, R.J., M.D. Weidmann, V.P. Sharma, and J.S. Condeelis. 2017. Tumor Cell Invadopodia: Invasive Protrusions that Orchestrate Metastasis. *Trends Cell Biol.* 27:595–607. https://doi.org/10.1016/j.tcb.2017.03.003

Jacob, A., and R. Prekeris. 2015. The regulation of MMP targeting to invadopodia during cancer metastasis. *Front. Cell Dev. Biol.* 3:4. https://doi.org/10.3389/fcell.2015.00004

Kelly, T., S.C. Mueller, Y. Yeh, and W.T. Chen. 1994. Invadopodia promote proteolysis of a wide variety of extracellular matrix proteins. *J. Cell. Physiol.* 158:299–308. https://doi.org/10.1002/jcp.1041580212

Linder, S., D. Nelson, M. Weiss, and M. Aepfelbacher. 1999. Wiskott-Aldrich syndrome protein regulates podosomes in primary human macrophages. *Proc. Natl. Acad. Sci. USA.* 96:9648–9653. https://doi.org/10.1073/pnas.96.17.9648

Linder, S., C. Wiesner, and M. Himmel. 2011. Degrading devices: invadosomes in proteolytic cell invasion. *Annu. Rev. Cell Dev. Biol.* 27:185–211. https://doi.org/10.1146/annurev-cellbio-092910-154216

Lochter, A., M.D. Sternlicht, Z. Werb, and M.J. Bissell. 1998. The significance of matrix metalloproteinases during early stages of tumor progression. *Ann. N. Y. Acad. Sci.* 857(1 MORPHOGENESIS):180–193. https://doi.org/10.1111/j.1749-6632.1998.tb10116.x

Mueller, S.C., Y. Yeh, and W.T. Chen. 1992. Tyrosine phosphorylation of membrane proteins mediates cellular invasion by transformed cells. *J. Cell Biol.* 119:1309–1325. https://doi.org/10.1083/jcb.119.5.1309

Murphy, D.A., and S.A. Courtneidge. 2011. The 'ins' and 'outs' of podosomes and invadopodia: characteristics, formation and function. *Nat. Rev. Mol. Cell Biol.* 12:413–426. https://doi.org/10.1038/nrm3141

Parrish, J.E., A. Ciccodicola, M. Wehhert, G.F. Cox, E. Chen, and D.L. Nelson. 1995. A muscle-specific DNase I-like gene in human Xq28. *Hum. Mol. Genet.* 4:1557–1564. https://doi.org/10.1093/hmg/4.9.1557

Paulick, M.G., and C.R. Bertozzi. 2008. The glycosylphosphatidylinositol anchor: a complex membrane-anchoring structure for proteins. *Biochemistry.* 47:6991–7000. https://doi.org/10.1021/bi8006324

Paz, H., N. Pathak, and J. Yang. 2014. Invading one step at a time: the role of invadopodia in tumor metastasis. *Oncogene.* 33:4193–4202. https://doi.org/10.1038/onc.2013.393

Poincloux, R., F. Lizárraga, and P. Chavrier. 2009. Matrix invasion by tumour cells: a focus on MT1-MMP trafficking to invadopodia. *J. Cell Sci.* 122:3015–3024. https://doi.org/10.1242/jcs.034561

Poulter, N.S., A.Y. Pollitt, A. Davies, D. Malinova, G.B. Nash, M.J. Hannon, Z. Pikramenou, J.Z. Rappoport, J.H. Hartwig, D.M. Owen, et al. 2015. Platelet actin nodules are podosome-like structures dependent on Wiskott-Aldrich syndrome protein and ARP2/3 complex. *Nat. Commun.* 6:7254. https://doi.org/10.1038/ncomms8254

Rafiq, N.B.M., Y. Nishimura, S.V. Plotnikov, V. Thiagarajan, Z. Zhang, S. Shi, M. Natarajan, V. Viasnoff, P. Kanchanawong, G.E. Jones, and A.D. Bershadsky. 2019. A mechano-signalling network linking microtubules, myosin IIA filaments and integrin-based adhesions. *Nat. Mater.* 18:638–649. https://doi.org/10.1038/s41563-019-0371-y

Raynaud-Messina, B., L. Bracq, M. Dupont, S. Souriant, S.M. Usmani, A. Proag, K. Pingris, V. Soldan, C. Thibault, F. Capilla, et al. 2018. Bone degradation machinery of osteoclasts: An HIV-1 target that contributes to bone loss. *Proc. Natl. Acad. Sci. USA.* 115:E2556–E2565. https://doi.org/10.1073/pnas.1713370115

Ridley, A.J. 2011. Life at the leading edge. *Cell.* 145:1012–1022. https://doi.org/10.1016/j.cell.2011.06.010

Saltel, F., T. Daubon, A. Juin, I.E. Ganuza, V. Veillat, and E. Génot. 2011. Invadosomes: intriguing structures with promise. *Eur. J. Cell Biol.* 90:100–107. https://doi.org/10.1016/j.ejcb.2010.05.011

Shiokawa, D., T. Matsushita, Y. Shika, M. Shimizu, M. Maeda, and S. Tanuma. 2007. DNase X is a glycosylphosphatidylinositol-anchored membrane enzyme that provides a barrier to endocytosis-mediated transfer of a foreign gene. *J. Biol. Chem.* 282:17132–17140. https://doi.org/10.1074/jbc.M610428200

Tarone, G., D. Cirillo, F.G. Giancotti, P.M. Comoglio, and P.C. Marchisio. 1985. Rous sarcoma virus-transformed fibroblasts adhere primarily at discrete protrusions of the ventral membrane called podosomes. *Exp. Cell Res.* 159:141–157. https://doi.org/10.1016/S0014-4827(85)80044-6

Uekita, T., Y. Itoh, I. Yana, H. Ohno, and M. Seiki. 2001. Cytoplasmic tail-dependent internalization of membrane-type 1 matrix metalloproteinase is important for its invasion-promoting activity. *J. Cell Biol.* 155:1345–1356. https://doi.org/10.1083/jcb.200108112

Van Goethem, E., R. Guiet, S. Balor, G.M. Charrière, R. Poincloux, A. Labrousse, I. Maridonneau-Parini, and V. Le Cabec. 2011. Macrophage podosomes go 3D. *Eur. J. Cell Biol.* 90:224–236. https://doi.org/10.1016/j.ejcb.2010.07.011

Wagenaar-Miller, R.A., L. Gorden, and L.M. Matrisian. 2004. Matrix metalloproteinases in colorectal cancer: is it worth talking about? *Cancer Metastasis Rev.* 23:119–135. https://doi.org/10.1023/A:1025819214508

Wang, Y., Y. Zhao, A. Sarkar, and X. Wang. 2019. Optical sensor revealed abnormal nuclease spatial activity on cancer cell membrane. *J. Biophotonics.* 12:e201800351. https://doi.org/10.1002/jbio.201800351

Winer, A., S. Adams, and P. Mignatti. 2018. Matrix Metalloproteinase Inhibitors in Cancer Therapy: Turning Past Failures Into Future Successes. *Mol. Cancer Ther.* 17:1147–1155. https://doi.org/10.1158/1535-7163.MCT-17-0646

Supplemental material

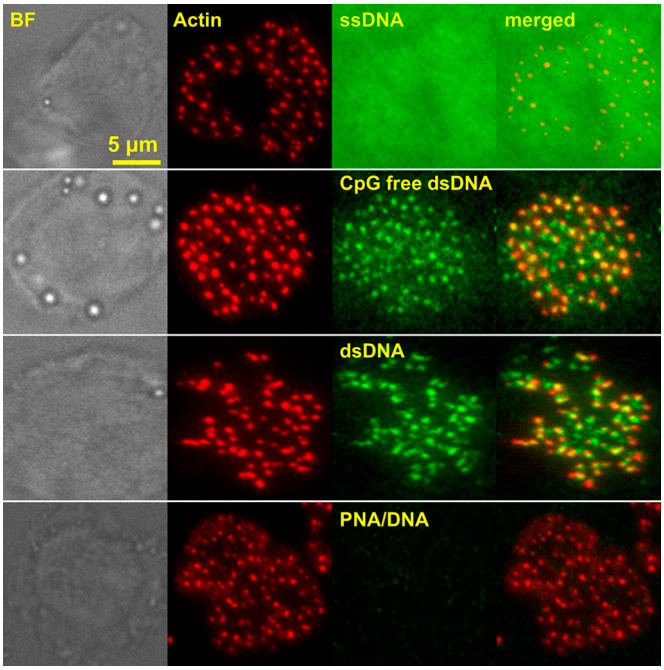

Figure S1. **DNase in podosomes does not degrade ssDNA but degrade dsDNA irrespective of their sequences.** THP-1 cells were plated on ssDNA, CpG-free dsDNA (CpG motif potentially stimulates immune response), dsDNA, and DNA–PNA modified surfaces. Podosomes (identified with an actin core) degraded dsDNA regardless of DNA sequences, but no degradation was exhibited on ssDNA or PNA–DNA hybrid. Refer to Materials and methods for the constructs of these DNA and PNA duplexes.

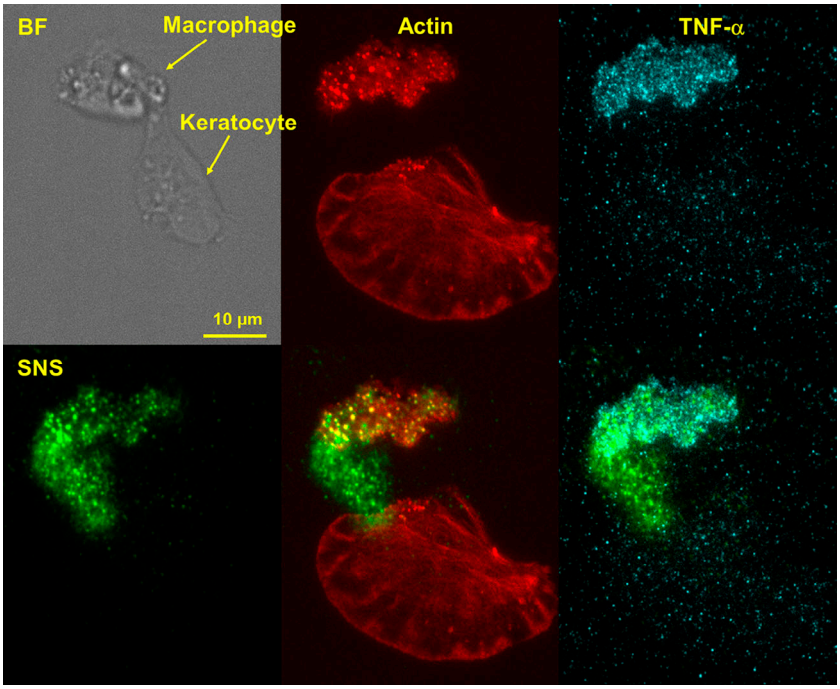

Figure S2. **Identification of fish macrophage and its DNase activity in the podosomes.** Cells harvested from fish scales consist of macrophages and keratocytes. The macrophage was identified with specific antibody (anti-TNF-α), and the expression of TNF-α was correlated with formation of podosomes and DNase activity. Therefore, one can distinguish macrophages from keratocytes simply by observing the SNS signal produced by cells. By estimate, ∼10–30% of cells harvested from fish scales are macrophages.

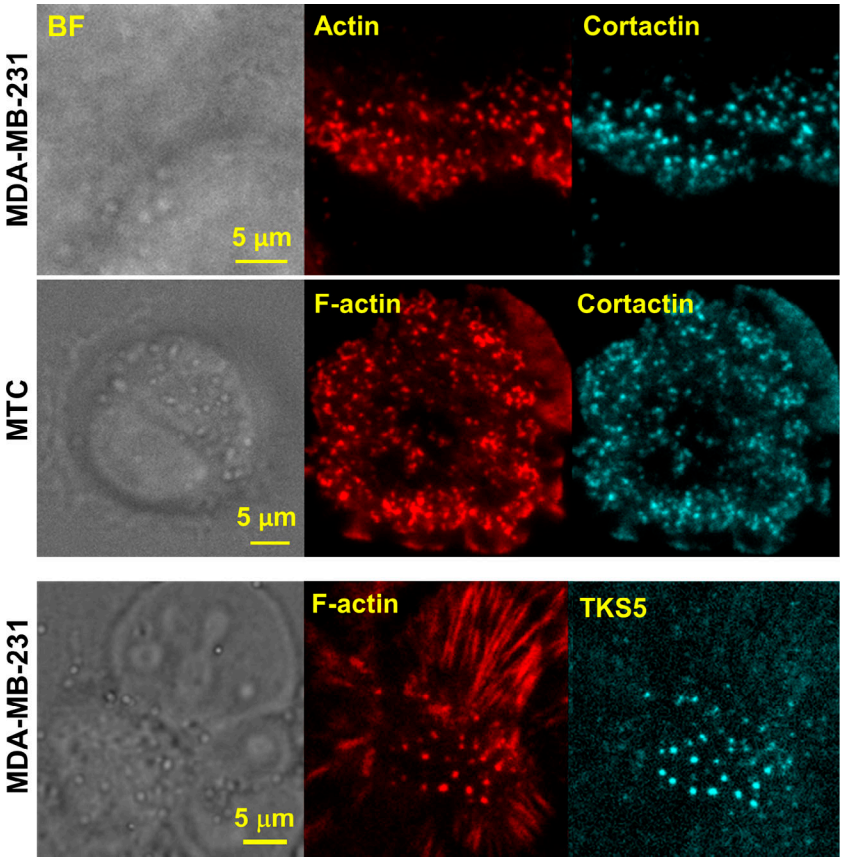

Figure S3. **Characterizing actin puncta as the invadopodia in two cancer cell lines.** Cancer cell line MTC and MDA-MB-231 had a number of punctate actin structures. These actin puncta were identified as invadopodia, as they were well colocalized with cortactin, as shown by immunostaining. In addition, in MDA-MB-231 cells, punctate F-actin structures are well colocalized with invadopodia marker TKS5.

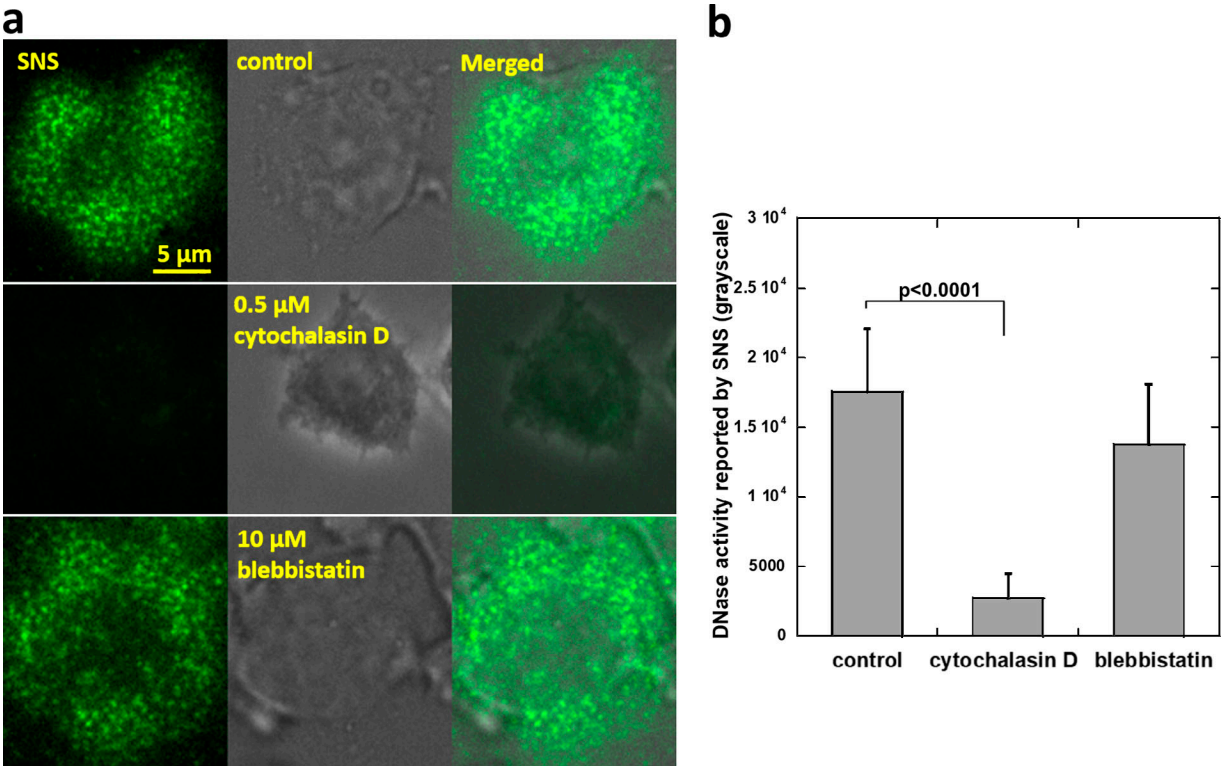

Figure S4. **Actin polymerization is required for DNase activity in podosomes. (a)** RAW264.7 cells were plated on SNS surfaces with actin polymerization inhibited by cytochalasin D or myosin II inhibited by blebbistatin. **(b)** The bar graph showed that the cytochalasin D significantly reduced the DNase activity in podosomes, whereas blebbistatin had a minor effect on DNase activity. 100 podosomes were analyzed for each data point. The significance (P value) was evaluated by two-tailed tests. Error bars represent SD.

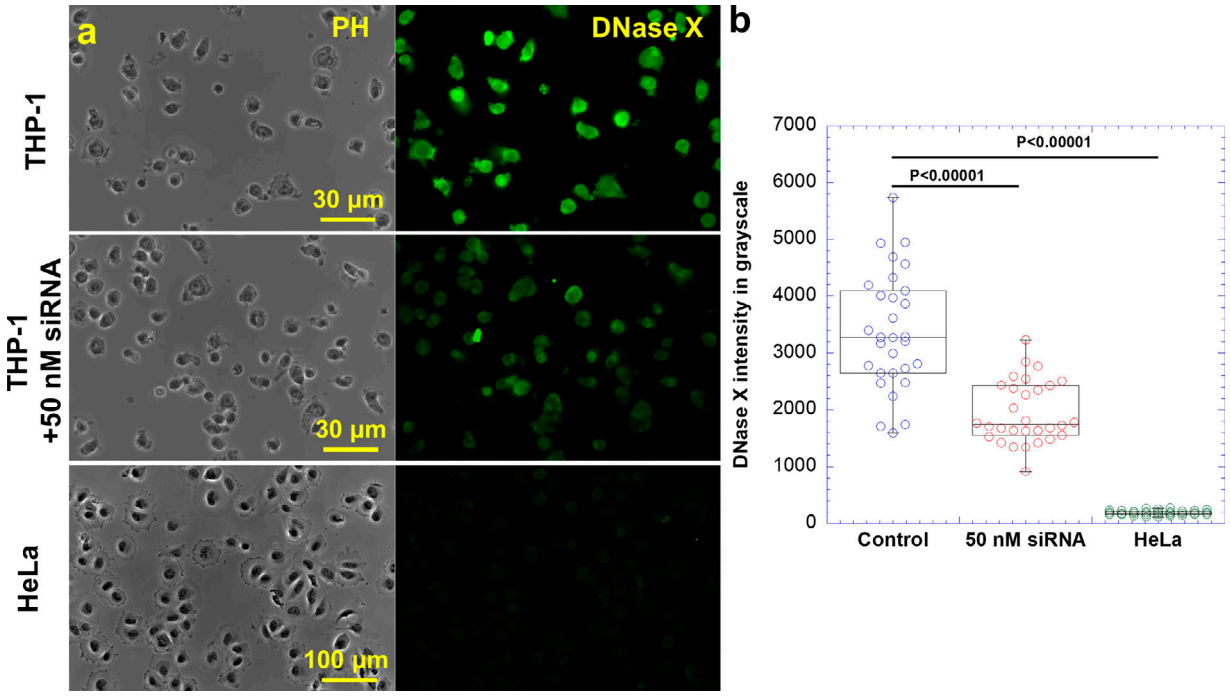

Figure S5. **Confirming siRNA-induced knockdown of DNase X by immunofluorescence. (a)** THP-1 cells pretreated with 50 nM nontargeting siRNA (positive control), THP-1 pretreated with 50 nM siRNA targeting DNase X, and HeLa cells (negative control) were immunostained with the anti-DNase X antibody and secondary fluorescent antibody. Cells were imaged by Epi-fluorescence microscopy that visualizes DNase X throughout cell bodies. **(b)** Fluorescence intensities of the images in grayscale values were measured for the quantification. $n = 30$. The result showed that the expression level of DNase X in THP-1 cells was significantly reduced by siRNA knockdown. All significance values (P values) were evaluated by two-tailed tests.

Video 1. **Coimaging of F-actin and DNase activity in a RAW264.7 cell on an SNS surface.** The video plays at 9 frames/s with a frame interval of 10 s in real time (20 min real time in total).

Video 2. **Podosomes in a THP-1 cell degraded DNA and FN.** The video plays at 9 frames/s with a frame interval of 30 s in real time (36 min real time in total).

Video 3. **Invadopodia in an MTC cell degraded DNA, but not FN, within the experiment time frame.** The video plays at 9 frame/s with a frame interval of 30 s in real time (36 min real time in total).

Video 4. **A migrating macrophage degrading extracellular DNA on an SNS surface by podosomes in the cell front.** The video plays at 6 frames/s with a frame interval of 30 s in real time (15 min real time in total).

Video 5. **A THP-1 cell reacted to *E. coli* by forming DNase-active podosomes around *E. coli*.** The video plays at 6 frames/s with a frame interval of 30 s in real time (30 min real time in total).

The MATLAB code developed for and used in this study is available online as Data S1.